Separation Science and Technology
Publication details, including instructions for authors and subscription information:
http://www.informaworld.com/smpp/title~content=t713708471

Effects of Air-Sparging on the Filtration Flux and Cake Properties in Cross-Flow Microfiltration of Size-Distributed Fine Particles

Kuo-Jen Hwang[a]; Shiau-Feng Wu[a]
[a] Department of Chemical and Materials Engineering, Tamkang University, Tamsui, Taipei Hsien, Taiwan

To cite this Article Hwang, Kuo-Jen and Wu, Shiau-Feng(2009) 'Effects of Air-Sparging on the Filtration Flux and Cake Properties in Cross-Flow Microfiltration of Size-Distributed Fine Particles', Separation Science and Technology, 44: 15, 3485 — 3505
To link to this Article: DOI: 10.1080/01496390903183345
URL: http://dx.doi.org/10.1080/01496390903183345

Separation Science and Technology, 44: 3485–3505, 2009

ISSN: 0149-6395 print/1520-5754 online
DOI: 10.1080/01496390903183345

Taylor & Francis
Taylor & Francis Group

Effects of Air-Sparging on the Filtration Flux and Cake Properties in Cross-Flow Microfiltration of Size-Distributed Fine Particles

Kuo-Jen Hwang and Shiau-Feng Wu
Department of Chemical and Materials Engineering, Tamkang University, Tamsui, Taipei Hsien, Taiwan

Abstract: The effect of air-sparging on the performance of cross-flow microfiltration of size-distributed fine particles is studied. The filtration flux and cake properties under various air velocities are measured and discussed. A higher air velocity leads to a lighter cake due to the higher shear stress acting on the membrane surface, especially under a bubble flow regime. However, the decrease in deposited particle size causes higher average specific cake filtration resistance as well as lower pseudo-steady filtration flux. A force balance model is employed to grasp the particle deposition on the membrane surface. The drag forces due to fluid flows play a major role in determining the particle deposition probability. The interparticle forces are dominant for submicron particles, while the inertial lift and gravitational force increase the weights for those particles larger than 10 μm. The occurrences of a minimum deposited probability for 0.2–0.3 μm particles and a maximum value for *ca* 2 μm particles can be reasonably explained by the force analysis. The particle size distribution in the filter cake, cake mass, average specific cake filtration resistance, and filtration flux can be estimated satisfactorily using theoretical models. In cross-flow microfiltration using a sample including submicron and micron particles, the filtration flux may be increased by sparging a few air bubbles. Air sparging is more effective in enhancing the filtration flux under lower suspension and air velocities due to the particle size effect. However, the flux-enhanced effectiveness decreases with increasing air velocity under bubble flow and becomes negative under a slug flow regime.

Received 4 March 2009; accepted 10 June 2009.

Address correspondence to Kuo-Jen Hwang, Department of Chemical and Materials Engineering, Tamkang University, Tamsui, Taipei Hsien 25137, Taiwan. Fax: +886-2-26209887. E-mail: kjhwang@mail.tku.edu.tw

Keywords: Cake properties, cross-flow microfiltration, gas-liquid flow pattern, particle deposition, solid-liquid separation

INTRODUCTION

Cross-flow filtration is a filtration mode in which the suspension flows tangentially across the membrane surface, while the filtrate permeates vertically. Since the shear stress acting on the membrane surface diminishes the cake growth, this kind of filtration always results in a much higher flux than dead-end filtration does. Therefore, cross-flow microfiltration has been increasingly used in industrial processes for separating fine particles, microbial cells, or colloids in recent years. However, membrane fouling due to particle deposition or molecular adsorption is a frequent serious problem in maintaining high filtration flux. Many anti-fouling strategies have been proposed to improve filtration flux or membrane selectivity, for instance, to generate a pulsation flow, vortex, increase turbulence, etc. (1). Coupling those concepts for producing turbulent perturbations, air bubbles were injected into the filter to reduce the cake growth and, certainly, to maintain the filtration flux as high as possible (2–9).

In previous studies, the filtration flux in air-sparging cross-flow microfiltration was correlated to the operating parameters into empirical equations (6,7) or analyzed based on hydrodynamic models (2–5,9). In general, the filtration flux can be enhanced under most conditions because the cake mass always decreases by sparging air bubbles. Cui and Wright (2,3) carried out the ultrafiltration of dextran, blue dextran, and BSA suspensions. They found that the fluxes in up and downward vertical filter tubes could be enhanced as high as 60 to 320-fold by injecting air bubbles. The shear stress, which plays the most important role on cake growth, depends significantly on air-liquid flow patterns. The wall shear stress generated under a slug flow is much higher than that under a bubble flow. Hence, operating microfiltration under a slug flow regime should be more effective in reducing particle deposition or membrane fouling. Lee et al. (8) claimed that the filtration flux increased 100% when the cross-flow ultrafiltration of *E. coli* operated under a slug flow regime. Mercier-Bonin and Fonade (5) indicated that the filtration flux in the cross-flow microfiltration of enzyme/yeast mixtures was improved 140% under a slug flow, but was only slightly increased in a bubble flow pattern. Although most previous studies indicated that the filtration flux was effectively enhanced by air-sparging, Cabassud et al. (9) showed experimentally that the maximum flux occurred at a specific air velocity in ultrafiltration using hollow fibers. They analyzed the hydrodynamic

parameter effects on the cake properties and claimed that the flux enhancement was controlled by the turbulence near the membrane surface. Recently, Hwang and co-workers (10,11) studied flux enhancement in the cross-flow microfiltration of uniform-sized fine particles and yeast cells using sparging air bubbles. They analyzed the shear stress acting on the membrane surface using gas-liquid two-phase flow models. Although the cake mass decreased with increasing shear stress, the marked increase in average specific cake filtration resistance due to particle compact packing may result in a lower flux in some occasions. They concluded that to perform microfiltration under a slug flow pattern was more effective in enhancing filtration flux.

Since most particulate products in industrial processes have a size distribution, the particle deposition probability is strongly dependent on the particle sizes. Therefore, the analyses in previous studies should be modified to take this effect into consideration when applying membrane filtration to industrial applications. In this article, air-sparging cross-flow microfiltration is performed using size-distributed fine particles whose diameters range from submicron to micron. The shear stress and particle deposition on the membrane surface are analyzed theoretically based on hydrodynamic models. The air velocity effects on the filtration flux and cake properties are measured and discussed.

THEORETICAL MODELS

Shear Stress Acting on the Membrane Surface

For a gas-liquid two-phase flow in a conduit, the flow pattern is dependent on the gas injection factor which is defined as (9):

$$\theta \equiv \frac{u_G}{u_G + u_L} \tag{1}$$

where u_G and u_L are the superficial velocities of the gas and liquid, respectively. A bubble flow, in which small air bubbles disperse uniformly in a liquid medium, occurs when $\theta < 0.2$. When $0.2 < \theta < 0.9$, the intermittent bullet-like large bubbles result in a slug flow. An annular flow, in which the liquid flows in a thin film near the conduit walls, occurs when $\theta > 0.9$.

For the two-parallel-plate microfilter used in this study, the shear stress acting on the membrane surface can be evaluated using a momentum balance on the filter channel (10), that is,

$$\tau_w = \frac{H}{2}\left(-\frac{dP_L}{dx}\right) \tag{2}$$

where H is the channel clearance. In the bubble flow regime, the pressure drop in the filter channel, $-dP_L/dx$, can be estimated using a liquid-gas two-phase flow model (10–12) by assuming the same friction factor value for both phases. On the other hand, large flattened air bubbles flow across the filter channel in the slug flow regime and the shear stress becomes intermittent. The mean wall shear stress can then be calculated by summing the stresses produced by the gas slugs, τ_{wG}, and the liquid slugs, τ_{wL}, that is (13),

$$\tau_w = \beta \cdot \tau_{wG} + (1 - \beta) \cdot \tau_{wL} \tag{3}$$

where β is the rate of intermittency, which is directly linked to the lengths of the long bubbles and the liquid slug. The shear stress produced by the liquid slugs can be estimated using the two-phase flow model (10–12), i.e., Eq. (2), while the τ_{wG} value can be calculated by assuming a linear velocity profile in the thin liquid film between the slug bubble and the membrane surface (14), that is,

$$\tau_{wG} = \mu_L \frac{u_L}{\delta} \tag{4}$$

where μ_L is the liquid viscosity and δ is the thickness of the liquid film between the air bubbles and the membrane surface. The film thickness can be accurately estimated using the following empirical equation if the Capillary number, Ca, is between 10^{-5} and 10^{-2} (15):

$$\delta = 1.337\left(\frac{H}{2}\right) Ca^{2/3} \tag{5}$$

The Capillary number is defined as:

$$Ca \equiv \frac{\mu_L v_b}{\gamma} \tag{6}$$

where v_b is the bubble velocity and y is the surface tension.

Force Balance Model for Particle Deposition

The external forces exerted on a depositing particle include the drag forces in the tangential and filtration directions, gravitational force, inertial lift force, and interparticle forces (11,16–18). The drag forces due to fluid flows always play the most important roles in determining the particle deposition among all forces. When the filtered particles have a wide size distribution, the interparticle forces are dominant

for submicron particles, while the gravitational and lift forces are important only when the particle size exceeds 10 μm (18). In general, the DLVO theory is used to estimate the interparticle forces for submicron particles.

The magnitude and direction of the net interparticle force are determined by summing the van der Waals and electrostatic forces. For the estimation of each force, refer to the authors' previous studies (10–11,16–18). For example, the drag force in the tangential direction can be evaluated using the modified Stokes law once the shear stress is known (10–11).

The force balance model derived in the authors' previous studies (16–18) is used to determine whether a particle can deposit stably onto the membrane surface or not. The external forces exerted on the particle are analyzed and divided into two directions, normal and tangential, to the line connecting the particle centers. The particle can deposit when the frictional force exceeds the net tangential force. The critical friction angle between particles, β_c can be estimated accordingly. A particle can deposit stably only if the friction angle is smaller than the critical value.

Considering the area in which the particles have the opportunity to deposit, the particle deposition probability, $P(d_p)$ can be estimated theoretically using (16,18)

$$P(d_p) = \frac{\beta_c}{\pi/2} \tag{7}$$

On the other hand, the particle deposition probability can also be obtained using a particle balance for those particles arriving at the membrane surface (16,18), that is,

$$P(d_p) = \frac{f_c(d_p)N_w}{f_o(d_p)N_b}. \tag{8}$$

where $f_c(d_p)$ and $f_o(d_p)$ are the frequency functions of the size d_p in the cake and the suspension, respectively. The particle mass flux arriving at the membrane surface, N_b, can be calculated using the product of the filtration flux and suspension concentration, while the mass flux of particle deposition, N_w, can be obtained from the tangent slope of the cake growth curve. Therefore, the particle deposition probability can be obtained by substituting the experimental data into the right-hand side of Eq. (8).

The particle size distribution in the cake can then be estimated once the deposited probability for each size is known. The cake mass

can then be calculated theoretically using the following time integration (16,18):

$$w_c = \int_0^t C_o \cdot q \cdot \left(\int_0^\infty f_o(d_p) \cdot P(d_p) d\ d_p \right) dt \tag{9}$$

where C_o is the suspension concentration and q is filtration flux.

Cake Property Estimation

The basic filtration equation can be written as

$$q = \frac{\Delta P}{\mu_L (w_c \cdot \alpha_{av} + R_m)} \tag{10}$$

where ΔP is the filtration pressure, w_c and α_{av} are the mass and average specific filtration resistance of cake, respectively, and R_m is the clean membrane resistance. Comparing Eq. (10) with the Kozeny-Carman equation for fluid flow through porous media, the average specific filtration resistance can be expressed as

$$\alpha_{av} = \frac{k S_o^2 \cdot (1 - \varepsilon)}{\rho_s \cdot \varepsilon^3} \tag{11}$$

where k is the Kozeny constant, S_o is the specific surface area of particles, ρ_s is the particle density, and ε is the cake porosity. For spherical particles under compact packing, the k value is equal to 5.0. The S_o value is equal to $6/d_p$ for a spherical particle with a diameter of d_p. However, when a spherical particulate sample has a size distribution, the S_o value should be evaluated using $6/d_{p,av}$ where $d_{p,av}$ is the particle mean diameter calculated based on the surface area. The cake porosity can be measured in experiments or calculated theoretically using a free cell model (19), that is,

$$\varepsilon = 1 - (1 - \varepsilon_o) \cdot \left(\frac{d_{p,av} + 2\sigma}{d_{p,av} + D} \right)^3 \tag{12}$$

where σ is the particle Stern layer thickness, D is the equilibrium distance between the neighboring particles in the cake, and ε_o is the porosity of the most compact cake ranging from 0.38 to 0.43 in general (19).

The average specific cake filtration resistance can be estimated theoretically using Eq. (11) once the k, S_o, and ε values are obtained.

Combining these values with the cake mass obtained in the previous section, the filtration flux for a given condition can then be predicted using Eq. (10).

MATERIALS AND METHODS

A particulate sample made of polymethyl methacrylate (PMMA) was used in this study. The particles were purchased from Soken Chemical & Engineering Co. in Japan. The density of the particulate sample was 1210 kg/m^3. A SEM photo for the sample is shown in Fig. 1(a). The particle shape was nearly spherical. The particle size distribution of

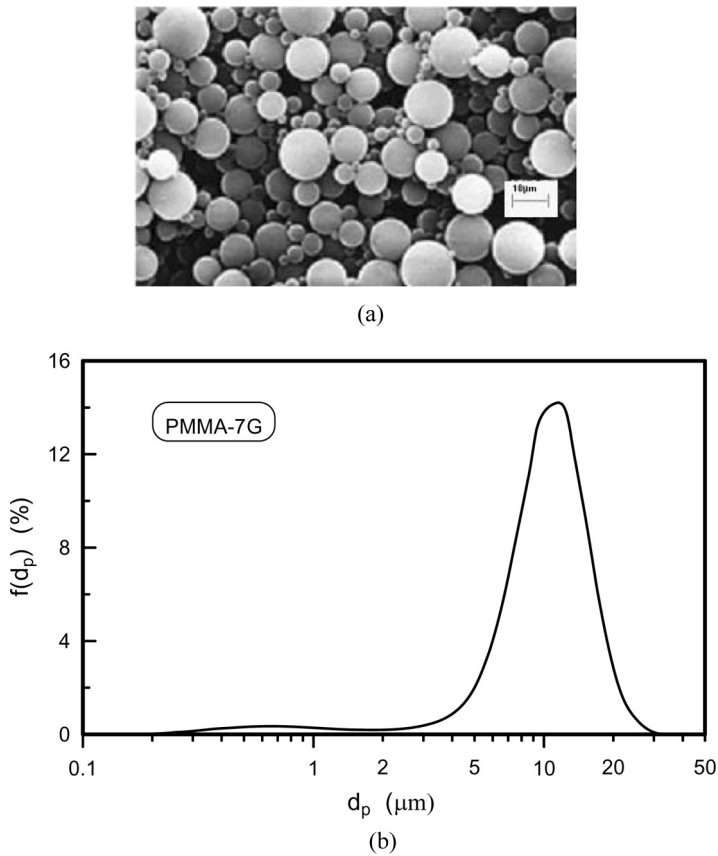

Figure 1. (a) SEM photo of the PMMA particulate sample. (x 2.0 kX); (b) Particle size distribution of the PMMA particulate sample.

the sample is shown in Fig. 1(b). Most particles had diameters ranging from 0.2 to 30 μm. The particles were suspended in de-ionized water to prepare the 0.01 wt% suspension used in these experiments. The particle zeta potential in such a condition was −32 mV. As a result, no particle coagulation occurred because of the high zeta potential. A filter membrane made of mixed cellulose ester and manufactured by ADVANTEC Micro Filtration Systems Co. was used in these experiments as the filter medium. The membrane mean pore size was 0.1 μm, and its filtration resistance was $2.52 \times 10^{11}\,m^{-1}$ under a pressure of 80 kPa.

Cross-flow microfiltration experiments were carried out using a two-parallel-plate microfilter. The filter channel clearance, width and length were 1.0×10^{-3} m, 2.0×10^{-2} m and 5.7×10^{-2} m, respectively. Since only the bottom plate was porous, the overall filtration area was $1.14 \times 10^{-3}\,m^2$. Figure 2 shows a schematic diagram of the cross-flow microfiltration system. The suspension was prepared and mixed well in a suspension tank. The pH and temperature were kept at 7.0 and 20°C, respectively, during filtration. The suspension was pumped into the filter using a peristaltic pump. Compressed air was injected into the filter channel and transported with the particle suspension. Cross-flow microfiltration experiments were performed under various suspension and air velocities and filtration pressures. The fluid velocities were controlled and measured using rotameters. The filtration pressure was adjusted

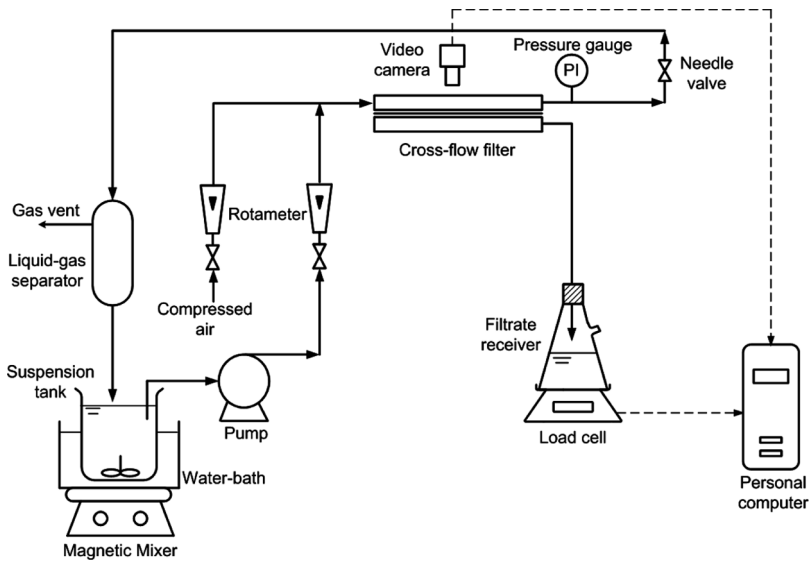

Figure 2. A schematic diagram of the cross-flow microfiltration system.

using a needle valve and indicated on the pressure gauge. The bubble sizes and shapes were observed using a video camera and recorded in a personal computer. All fluid flows in the operating conditions used in this study were laminar. The filtrate was collected into a receiver. Its weight was measured using a load cell and recorded on a personal computer through an RS-232 connection. The same amount of make-up water as the filtrate was duly added into the suspension tank to maintain a constant suspension concentration during filtration. When an experiment was terminated, the cake formed on the filter membrane was sent to analyze its wet and dry masses using an *ORION* moisture titrator, the particle size distribution using a *HORIBA LA-910* laser particle sizer, or packing structure using SEM after a liquid nitrogen quenching. Therefore, the average cake porosity and average specific cake filtration resistance could be calculated using the material balance and basic filtration equation, respectively.

RESULTS AND DISCUSSION

Figure 3 shows the filtration flux time courses under various air flow rates. The suspension velocity and filtration pressure were kept under 0.1 m/s and 20 kPa, respectively. The filtration flux attenuates rapidly

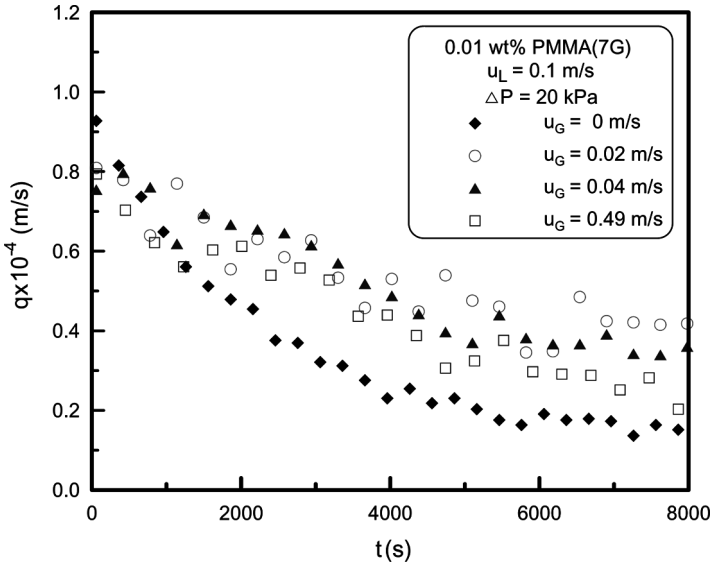

Figure 3. Time courses of filtration flux under various air flow rates.

at the beginning of filtration and then gradually approaches a pseudo-steady value after 4,000 seconds. This is because the cake growth is limited by the tangential suspension and air-bubble flows. Compared with no air-sparging conditions, more scattered data were found when air bubbles existed. This may be due to the intermittent and random bubble flows. The filtration flux can be enhanced by air-sparging. However, an excessive air velocity produces unexpected results in the lower filtration flux. This trend is possible due to the variations in the flow pattern (9,11) or in cake properties (18) and will be discussed below.

Figure 4 shows the suspension and air velocity effects on the pseudo-steady filtration flux. Because of data scattering, the pseudo-steady filtration fluxes shown in this figure are the average values between 6,000 and 8,000 s. In no air-sparging conditions, the flux increases with increasing suspension velocity. This is attributed to less cake formation under higher wall shear stress. The flux may be markedly increased by sparging a few air bubbles into the filter channel to increase the wall shear stress. However, a converse result is obtained as the air velocity is further increased and the air-sparging effect becomes trivial as the air velocity exceeds 0.1 m/s. The data also reveals that a lower suspension velocity, e.g., $u_L = 0.1$ m/s, is possible, resulting in a higher flux under the same air flow rate. Since the wall shear stress increases

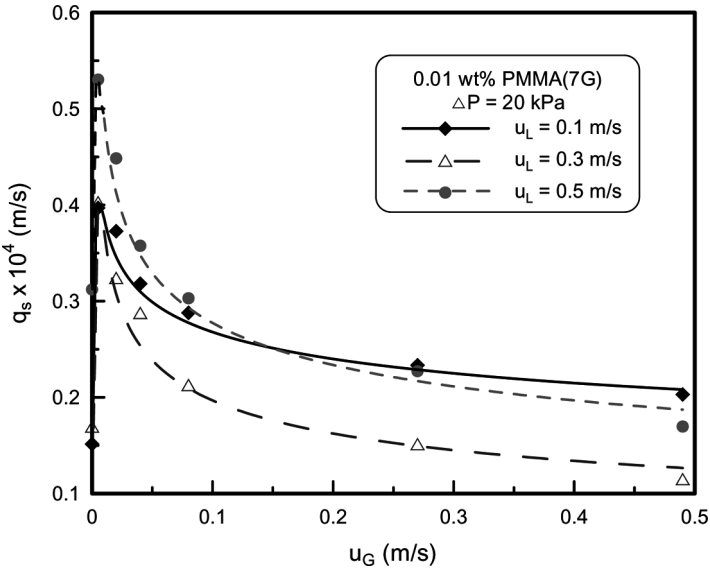

Figure 4. Effects of suspension and air velocities on the pseudo-steady filtration flux.

monotonously with increasing fluid velocities, it may not be the sole effect on the filtration flux. These irregular results imply that the cake properties, such as cake mass, porosity, and specific filtration resistance, play significant roles in determining the filtration performance. The variations in cake properties under various conditions should be analyzed prior to explaining the results shown in Fig. 4.

The air-sparging effectiveness for flux enhancement, r, is defined as the air-sparging flux ratio to no air-sparging conditions. Therefore, the filtration flux can be enhanced by air-sparging if $r > 1$. The r values under various suspension and air velocities are shown in Fig. 5. The maximum effectiveness occurs under an extremely low air velocity and then decreases with increasing air velocity. The decrease in r value becomes tiny as $u_G > 0.1\,\mathrm{m/s}$. The dashed line shown in Fig. 5 indicates the flow patterns under various conditions. The data shows in which the r value significantly decreases with increasing u_G in the bubble flow regime, but becomes insensitive, actually, a slight decrease in the slug flow regime. Since the r value increases with decreasing suspension velocity, air-sparging is more effective in enhancing filtration flux under lower suspension velocity. The r value is smaller than 1.0 when $u_G > 0.1\,\mathrm{m/s}$ and $u_L > 0.3\,\mathrm{m/s}$. This opposite tendency was not observed in previous

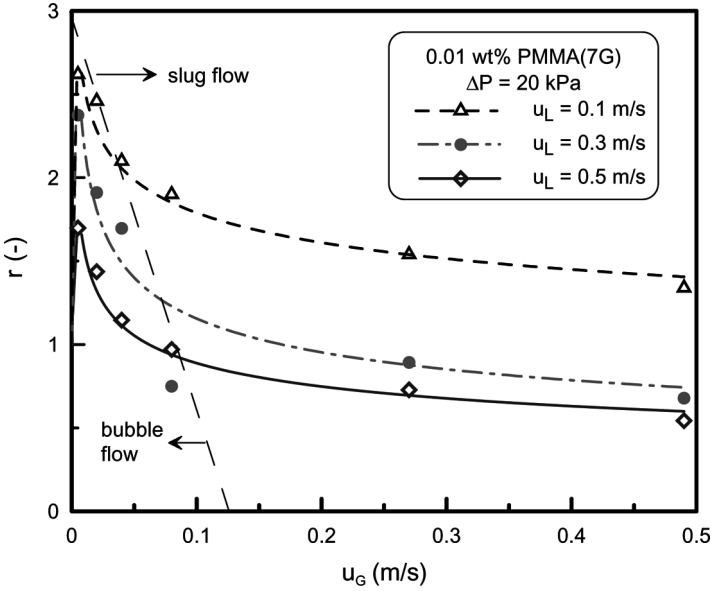

Figure 5. Effects of suspension and air velocities on the flux enhanced effectiveness.

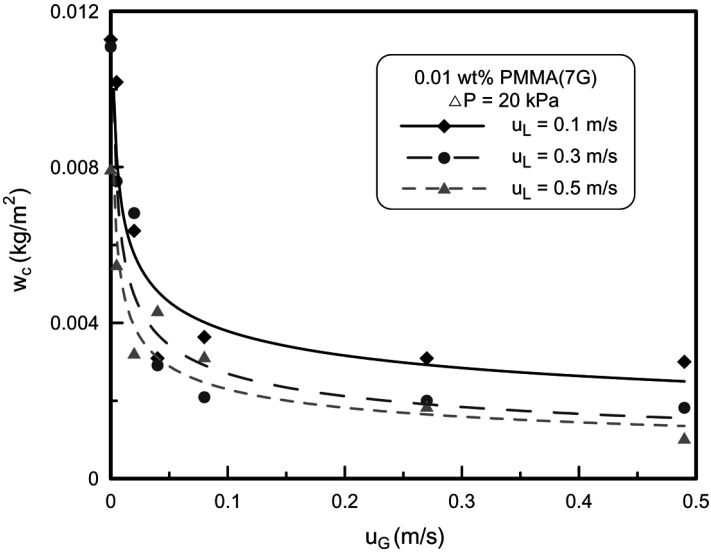

Figure 6. Effects of suspension and air velocities on the cake mass.

studies and is probably due to the particle size effect, which will be discussed in this study.

Figure 6 shows the cake masses in cross-flow microfiltration under various suspension and air velocities. The cake mass decreases with increasing gas velocity due to higher wall shear stress. Compared with the no air-sparging condition data ($u_G = 0$), over 60% of the cake mass can be diminished by air sparging under optimal conditions. However, this cake diminishing effect is more significant under bubble flows. The cake mass under a slug flow is almost invariant with air velocity. This result indicates that the cake mass diminished by air-sparging has an ultimate limitation and was also observed in the same operations for uniform-sized fine particles (10) and yeast cells (11). In addition, a lighter cake is formed under a higher suspension velocity. This can be expected since less cake is formed under a higher shear stress. However, some cake mass data under lower u_L are smaller than those under higher u_L when u_G ranges from 0.04 to 0.08 m/s. This is because the flow pattern under lower suspension velocities has been transformed into slug flows and generates higher wall shear stresses.

Figure 7 shows the air-sparging effect on the particle size distribution in the filter cake. The original PMMA-7 G particle size distribution in the suspension is also shown for comparison. The particle frequency functions shown in the figure were measured using a laser particle sizer. Since

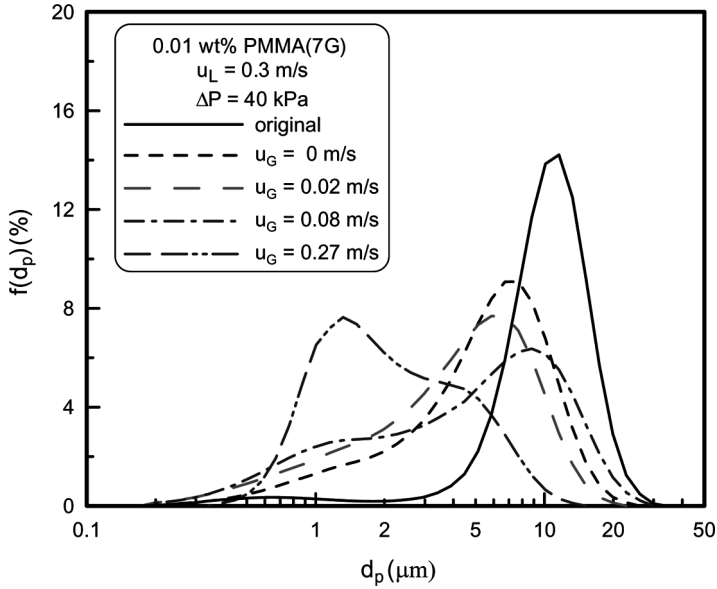

Figure 7. Effect of air velocity on the particle size distribution in the cake under $u_L = 0.3\,\mathrm{m/s}$ and $\Delta P = 40\,\mathrm{kPa}$.

the acting shear stress causes smaller particles to be more stable on the membrane surface, all particle size distributions in cakes are smaller than that in the suspension. In the no air-sparging condition, the mean particle diameter decreases from 10 μm in the suspension to *ca* 6 μm under $u_L = 0.3\,\mathrm{m/s}$ and $\Delta P = 40\,\mathrm{kPa}$. When air bubbles are sparged into the filter channel, the particle size distribution in the cake becomes even smaller under the bubble flow regime, e.g., $u_G = 0.02\,\mathrm{m/s}$, because of the increase in the wall shear stress. However, when the air velocity is increased further, the particle size distribution becomes wider under the slug flow regime. This may be due to the intermittent flow and bubble size distribution. Because the particles that can stably deposit onto the membrane surface become less as the air velocity increases, the decrease in cake mass under higher air velocity, as shown in Fig. 6, is due to the higher wall shear stress and also to the rare small particles.

According to the description in previous sections, the particle deposition probability can be calculated theoretically using Eq. (7) or calculated from the experimental data using Eq. (8). Figure 8 shows a comparison of particle deposition probability between the theoretical calculation and experimental data under three different air velocities. The curve trend is similar to that in the no air-sparging condition (18). The probability

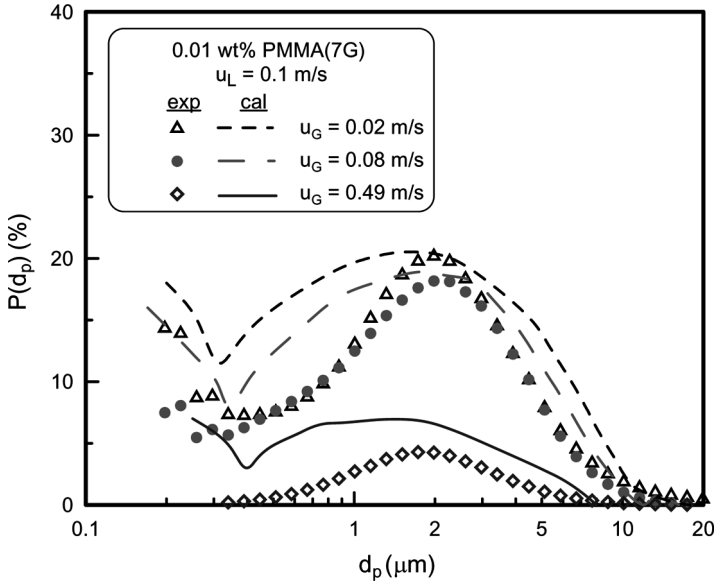

Figure 8. A comparison of particle deposition probability between calculated results and experimental data under various air velocities.

decreases and then increases with increasing particle diameter for submicron particles, reaches the maximum value for particles around 2–3 μm, and then decreases quickly until zero for particles about 10–20 μm in diameter. This trend can be explained reasonably using the force analysis in the authors' previous study (18). Since the interparticle forces are dominant for submicron particles, the minimum deposited probability occurring in the submicron region is because the net interparticle force changes from repulsive to attractive at *ca* 0.3–0.4 μm. When the particle size is larger than 1 μm, the weight of the interparticle forces decreases markedly, and the deposition probability increases with particle size due to the decrease in the drag force ratio in the tangential to filtration direction. As a result, the maximum deposition probability occurs at a diameter *ca* 2 μm. For larger particles, the inertial lift force quickly increases its weight among all external forces and reduces the deposition probability. The particles whose sizes exceed 10 μm have difficulty staying on the membrane surface in the operating conditions in this study. Comparing the data shown in Fig. 8, the particle deposition probability decreases with increasing air velocity. This is because the sparged air bubbles increase the wall shear stress and result in an extra sweeping force decreasing the particle stability. An agreement between the calculated

probability values and experimental data can be found in the figure. The larger deviation occurring in the submicron region under $u_G = 0.49\,\mathrm{m/s}$ may be due to the hard measurement for small particle amount.

Once the particle deposition probability is estimated, the cake mass can be evaluated theoretically by employing Eq. (9). Figure 9 shows a comparison of the cake mass between the calculated results and experimental data under various air velocities. The suspension velocity and filtration pressure were under 0.1 m/s and 20 kPa, respectively. The calculated cake mass agrees very well with experimental data in the bubble flow regime. The decrease in cake mass by increasing the air velocity can be accurately predicted. However, an overestimation occurs when $u_G > 0.1\,\mathrm{m/s}$ because of the overestimation in particle deposition probability in the slug flow regime, as shown in Fig. 8.

Figure 10 depicts the air velocity effect on the mean particle diameter in cake, $d_{p,av}$. The values for $d_{p,av}$ were calculated using the particle size distribution based on the surface area. The calculated mean particle diameters slightly decrease with increasing air velocity, while the experimental data shows scattered values. This reveals that finer particles deposit onto the membrane surface as the air velocity increases. The deviations between the calculated mean diameter and experimental data are less than 15%, as shown in the figure. This agreement indicates that the mean particle size in the cake can be accurately estimated using the proposed method.

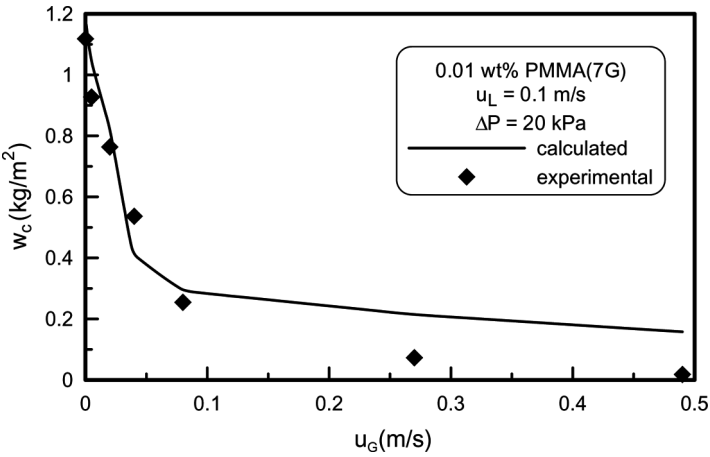

Figure 9. A comparison of cake mass between calculated results and experimental data.

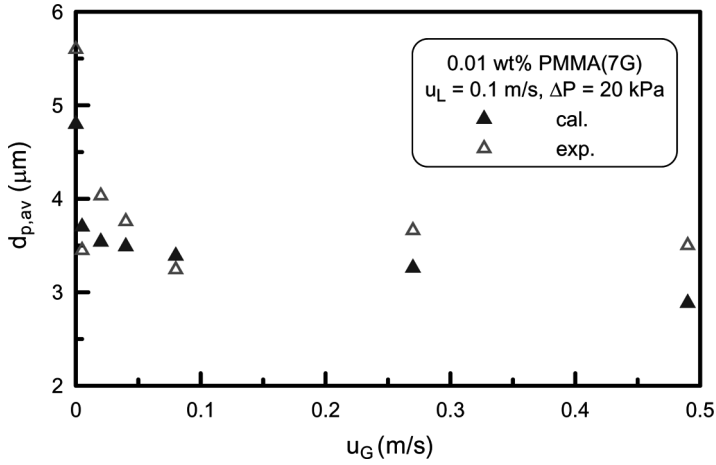

Figure 10. Comparison of the mean particle size in cake between calculated results and experimental data under various air velocities.

A comparison of the average specific cake filtration resistance, α_{av}, between the calculated results using Eq. (11) and experimental data under $u_L = 0.1$ m/s and $\Delta P = 20$ kPa is shown in Fig. 11. Since the particle packing structure becomes more compact (as indicated in the authors' previous studies (10,11)) and the particle size distribution in the cake becomes finer (or the particle specific surface area becomes larger) under higher air flow

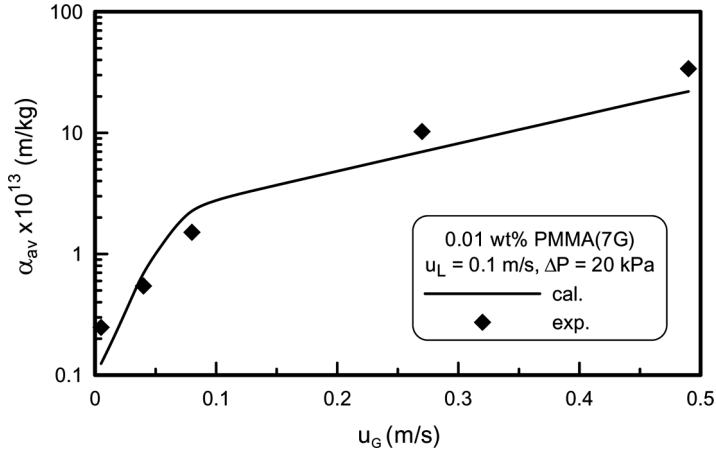

Figure 11. Comparison of average specific cake filtration resistance between calculated results and experimental data under various air velocities.

rate, the average specific cake filtration resistance increases significantly with increasing air velocity. When the air velocity increases, the significant decrease in the mean particle diameter and porosity in the cake under the bubble flow regime leads to a marked increase in α_{av}. It can be found that the order of magnitude of α_{av} increases from 10^{12} to $10^{14}\,m^{-1}$ when u_G increases from 0 to 0.5 m/s. The cake filterability changes from moderate to hard to filter due to air-sparging. This reveals that the cake properties, such as particle size distribution and packing structure, are significantly affected by sparging air bubbles. The huge increase in α_{av} implies that the filtration performance is not consequentially improved by air-sparging. An unexpected lower filtration flux may be obtained under higher air or suspension velocity, as shown in Fig. 4. However, an agreement between calculated α_{av} and experimental data is shown in Fig. 11. This demonstrates that the average specific cake filtration resistance can be estimated satisfactorily using the proposed method.

According to the basic filtration equation, Eq. (10), the α_{av} and w_c values should be analyzed prior to obtaining the filtration flux. Since the α_{av} value increases while the w_c value decreases as the air velocity increases (refer to Figs. 9 and 11), the air velocity effect on the filtration flux is determined using the product $\alpha_{av} \times w_c$. In some cases, e.g., the cross-flow microfiltration of uniform-size PMMA particles in the study of Hwang and Wu (10), the filtration flux is enhanced by increasing air velocity. However, contrary results may be found in other studies (9,11). Figure 12 shows a comparison of the filtration flux between the results calculated using Eq. (10) and experimental data under various

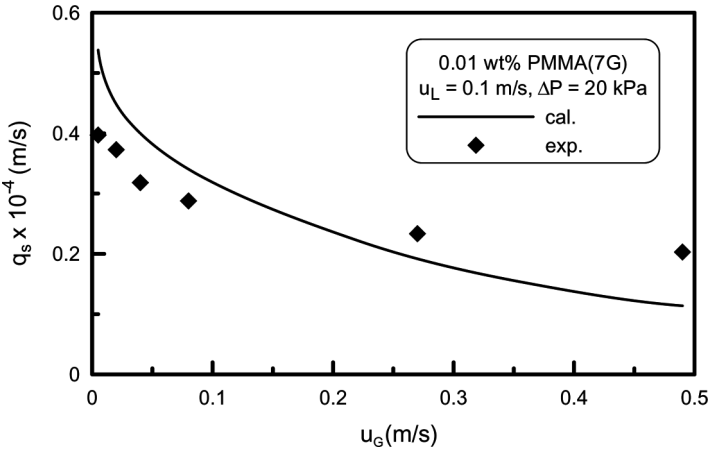

Figure 12. A comparison of pseudo-steady filtration flux between calculated results and experimental data under various air velocities.

air velocities. They have the same trends, an increase in air velocity leads to a lower filtration flux. This implies that the specific cake filtration resistance effect (or the particle size distribution in cake) is dominant in the operating conditions used in this study. However, a deviation as large as 30% between the calculated results and experimental data occurs, especially under a very low air velocity. This is attributed to the noticeable underestimation for α_{av} occurring under such low air flow rate. Furthermore, the filtration flux is underestimated when $u_G > 0.4\,\mathrm{m/s}$ because of the cake mass overestimation. The data shown in Fig. 12 also indicates that a 60% flux reduction may be obtained under a high air-sparging rate.

CONCLUSIONS

Air bubbles were sparged into the filter channel of a cross-flow microfilter to improve the filtration performance. The results indicated that a higher sparged air velocity led to a lighter cake due to the higher shear stress acting on the membrane surface. However, the smaller particle size in the cake caused a higher average specific cake filtration resistance and lower pseudo-steady filtration flux. A force balance model was employed to estimate the particle deposition probability and the particle size distribution in the filter cake. The filter cakes were constructed of finer particles under higher suspension or air velocities. The interparticle force domination for submicron particles caused a minimum deposited probability occurring at 0.2–0.3 μm, while the noticeable weight of the lift force for micron particles resulted in a maximum deposited probability occurring at *ca* 2 μm. The mean particle size in the filter cake, average specific cake filtration resistance, and filtration flux were predicted using hydrodynamic models. Satisfactory agreements between the calculated results and experimental data were obtained. The flux enhanced effectiveness decreased with air velocity in the bubble flow and became negative in the slug flow regime.

ACKNOWLEDGEMENTS

The authors wish to express their sincere gratitude to the National Science Council of the Republic of China for its financial support.

NOTATIONS

C_o	suspension concentration ($\mathrm{kg/m^3}$)
Ca	Capillary number defined by Eq. (6) (−)

D	equilibrium distance between neighbor particles in cake (m)
d_p	diameter of particles (m)
$d_{p,av}$	the particle mean diameter calculated based on the surface area (m)
$f_c(d_p)$	the frequency function of the size d_p in the cake (%)
$f_o(d_p)$	the frequency function of the size d_p in the suspension (%)
H	the clearance of the filter channel (m)
k	Kozeny constant (−)
N_b	particle mass flux arriving at the membrane surface ($kg/m^2 s$)
N_w	mass flux of particle deposition ($kg/m^2 s$)
P_L	hydraulic pressure (N/m^2)
$P(dp)$	particle deposition probability (%)
ΔP	filtration pressure (N/m^2)
q	filtration flux ($m^3/m^2 s$)
q_s	pseudo-steady state filtration flux ($m^3/m^2 s$)
r	air-sparging effectiveness for filtration flux enhancement (−)
R_m	filtration resistance of membrane (m^{-1})
So	specific surface area of particles (m^2/m^3)
t	filtration time (s)
u	superficial velocity (m/s)
v_b	bubble velocity (m/s)
w_c	cake mass per unit area (kg/m^2)
x	distance from the filter channel inlet in the suspension flow direction (m)

Greek Letters

α_{av}	average specific filtration resistance of cake (m/kg)
β	rate of intermittency (−)
β_c	critical friction angle between particles (rad)
ε	average cake porosity (−)
ε_o	porosity of the most compact cake (−)
δ	liquid film thickness (m)
γ	surface tension (N/m)
μ_L	filtrate viscosity (kg/s m)
θ	gas injection factor defined in Eq. (1) (−)
ρ_s	particle density (kg/m^3)
σ	particle Stern layer thickness (m)
τ_w	shear stress acting on the membrane surface (N/m^2)

Subscripts

G	gas
L	liquid

REFERENCES

1. Belfort, G.; Davis, R.H.; Zydney, A.L. (1994) The behavior of suspensions and macromolecular solutions in crossflow microfiltration. *J. Membr. Sci.*, *96*: 1–58.
2. Cui, Z.F.; Wright, K.I.T. (1994) Gas-liquid two phase flow ultrafiltration of BSA and dextran solutions. *J. Membr. Sci.*, *90*: 183–189.
3. Cui, Z.F.; Wright, K.I.T. (1996) Flux enhancements with gas sparging in downwards crossflow ultrafiltration: Performances and mechanisms. *J. Membr. Sci.*, *117*: 109–116.
4. Mercier-Bonin, M.; Lagane, C.; Fonade, C. (2000) Influence of a gas/liquid two-phase flow on the ultrafiltration and microfiltration performances: Case of a ceramic flat sheet membrane. *J. Membr. Sci.*, *180*: 93–102.
5. Mercier-Bonin, M.; Fonade, C. (2002) Air-sparged microfiltration of enzyme/yeast mixtures: Determination of optimal conditions for enzyme recovery. *Desalination*, *148*: 171–176.
6. Mikulášek, P.; Pospišil, P.; Dolecek, P.; Cakl, J. (2002) Gas-liquid two-phase flow in microfiltration mineral tubular membranes: Relationship between flux enhancement and hydrodynamic parameters. *Desalination*, *146*: 103–109.
7. Pospišil, P.; Wakeman, R.J.; Hodgson, I.O.A.; Mikulášek, P. (2004) Shear stress-based modelling of steady state permeate flux in microfiltration enhanced by two-phase flows. *Chem. Eng. J.*, *97*: 257–263.
8. Lee, C.K.; Chang, W.G.; Ju, Y.H. (1993) Air slugs entrapped cross-flow filtration of bacterial suspensions. *Biotechnol. Bioeng.*, *41*: 525–530.
9. Cabassud, C.; Laborie, S.; Durand-Bourlier, L.; Lainé, J.M. (2001) Air sparging in ultrafiltration hollow fibers: Relationship between flux enhancement, cake characteristics and hydrodynamic parameters. *J. Membr. Sci.*, *181*: 57–69.
10. Hwang, K.J.; Wu, Y.J. (2008) Flux enhancement and cake formation in air-sparged cross-flow microfiltration. *Chem. Eng. J.*, *139* (2): 296–303.
11. Hwang, K.J.; Hsu, C.E. (2009) Effect of gas-liquid flow pattern on air-sparged cross-flow microfiltration of yeast suspension. *Chem. Eng. J.*, *151*: 160–167.
12. Wilkes, J.O. (2006) *Fluid Mechanics for Chemical Engineers*, Chap. 10; Prentice Hall: New Jersey, USA, p. 468–474.
13. Mercier-Bonin, M.; Gésan-Guiziou, G.; Fonade, C. (2003) Application of gas/liquid two-phase flows during crossflow microfiltration of skimmed milk under constant transmembrane pressure conditions. *J. Membr. Sci.*, *218*: 93–105.
14. Briceño, M.I.; Joseph, D.D. (2003) Self-lubricated transport of aqueous foams in horizontal conduits, Intern. *J. Multiphase Flow*, *29*: 1817–1831.
15. Bretherton, F.P. (1961) The motion of long bubbles in tubes. *J. Fluid Mech.*, *10*: 166–188.
16. Lu, W.M.; Hwang, K.J. (1995) Cake formation in 2-D cross-flow filtration. *A.I.Ch.E. J.*, *41* (6): 1443–1455.
17. Hwang, K.J.; Lin, K.P. (2002) Cross-flow microfiltration of dual-sized submicron particles. *Sep. Sci. Technol.*, *37*: 2231–2249.

18. Hwang, K.J.; Hsu, Y.L.; Tung, K.L. (2006) Effect of particle size on the performance of cross-flow microfiltration. *Adv. Powder Technol.*, *17* (2): 189–202.
19. Hwang, K.J.; Liu, H.C.; Lu, W.M. (1998) Local properties of cake in cross-flow microfiltration of submicron particles. *J. Membr. Sci.*, *138*: 181–192.